Journal of Molecular Liquids 413 (2024) 126018

Contents lists available at ScienceDirect

Journal of Molecular Liquids

journal homepage: www.elsevier.com/locate/molliq

Facet engineering in cadmium sulfide for efficient reduction-recovery of low-concentration gold(I) from thiosulfate solutions

Jiabei Gao [a,b], Weiquan Zhan [c,d,*], Ziwei Xiang [b], Shaoxian Song [e], José Luis Arauz-Lara [d], Feifei Jia [a,b], Peng Chen [a,b,**]

[a] Key Laboratory of Green Utilization of Critical Non-metallic Mineral Resources of Ministry of Education, Wuhan, Hubei 430070, China
[b] School of Resources and Environmental Engineering, Wuhan University of Technology, Wenzhi Street 34, Wuhan 430070, Hubei, China
[c] Department of Mining and Minerals Engineering, Virginia Polytechnic Institute and State University, Blacksburg, VA 24061, United States
[d] Instituto de Física, Universidad Autónoma de San Luis Potosí, Av. Manuel Nava 6, Zona Universitaria, San Luis Potosí 78290, Mexico
[e] Instituto de Metalurgia, Universidad Autónoma de San Luis Potosí, Av. Sierra Leona 550, San Luis Potosí 78210, Mexico

ARTICLE INFO

Keywords:
Facet engineering
Cadmium sulfide
Reduction-recovery
Low-concentration
$Au(S_2O_3)_2^{3-}$

ABSTRACT

Trace gold(I) recovery from thiosulfate solutions limits the application of thiosulfate leaching instead cyanide leaching method in industries. Here, facet engineering in cadmium sulfide (CdS) was proposed for trace gold(I) recovery from thiosulfate solutions ($Au(S_2O_3)_2^{3-}$). CdS nanomaterials with various exposing facets were obtained through adjusting the sulfur sources in hydrothermal synthesis process. It was found that $Au(S_2O_3)_2^{3-}$ recovery could reach 98.62 % under low concentration conditions, with a max reduction capacity of 204.95 mg/g. Besides, the recovery form of $Au(S_2O_3)_2^{3-}$ on CdS was metallic gold, realizing the reduction and recovery at the same time. The solution pH, sample dosage, $S_2O_3^{2-}$, SO_3^{2-}, and ammonia ions as variants were considered to optimize the recovery performances. Even under the existence of interfered ions, the recovery kept very high. Au $(S_2O_3)_2^{3-}$ reduction on CdS was attributed to catalytic and chemical reduction. High exposed (002) facet content of CdS enhanced photocurrent intensity, thus improving $Au(S_2O_3)_2^{3-}$ reduction and recovery. Therefore, the work paved a way to realize trace gold(I) recovery from thiosulfate solutions via structure engineering in CdS, being expected to promote the application of thiosulfate leaching method.

1. Introduction

Gold (Au) with excellent high-temperature resistance [1], stability [2], and ductility [3] was widely used in aerospace [4], medical equipment [5], electronic industry [6] and other fields [7]. The extraction of gold came from various resources, but primarily gold ores [8] and urban mines [9]. At present, the main leaching method in faculties is cyanide leaching, which occupies about 90 % [10]. However, the well-known toxic cyanide-contained substances were produced during leaching process, extremely polluting ecosystems and endangering human health [11]. Therefore, it is urgent to develop non-cyanide leaching method for green recovery of gold.

Currently, non-cyanide leaching ways include thiourea [12], cupric chloride [13], ammonia [14], thiosulfate [15,16] leaching method, etc. Among these methods, the advantages of thiosulfate leaching were its environmental protection [17], fast leaching rate [18], and relatively low operating cost [19], while avoiding toxic chemicals. Nevertheless, the difficulty in recovering low-concentration gold complex ion ($Au(S_2O_3)_2^{3-}$) from thiosulfate leaching solution had become a significant technical bottleneck [20].

Typical gold recovery methods were solvent extraction [21], ion exchange [22], and cementation [23], adsorption [24], while they were hardly applied in actual $Au(S_2O_3)_2^{3-}$ recovery because of high cost, or low recovery. Besides, whatever using which recovery way, the leaching methods are three steps, adsorption, desorption, and reduction [25]. Recently, reduction-recovery method [26] based on catalysis is proposed to realize adsorption and reduction of $Au(S_2O_3)_2^{3-}$ together. Unsatisfactory, the recovery of low-concentration $Au(S_2O_3)_2^{3-}$ through reduction-recovery had not been researched.

Cadmium sulfide (CdS) with abundant surficial sulfur atoms was

* Corresponding author at: Department of Mining and Minerals Engineering, Virginia Polytechnic Institute and State University, Blacksburg, VA 24061, United States.
** Corresponding author at: Key Laboratory of Green Utilization of Critical Non-metallic Mineral Resources of Ministry of Education, Wuhan, Hubei 430070, China.
E-mail addresses: zhan_weiquan@163.com (W. Zhan), peng141592@163.com (P. Chen).

https://doi.org/10.1016/j.molliq.2024.126018
Received 13 April 2024; Received in revised form 6 September 2024; Accepted 13 September 2024
Available online 16 September 2024

prone to adsorb gold complex ions according to Hard-Soft-Acid-Base theory [27]. In addition, CdS could make better use of visible light due to its narrow band gap (2.4 eV) [28], thus playing an important role in catalytic reaction. The conduction band of CdS [29] was lower than the reduction potential of $Au(S_2O_3)_2^{3-}/Au^0$(0.15 eV) [30], which was prone to reduce $Au(S_2O_3)_2^{3-}$ into Au^0. Herein, it was expected to achieve reduction-recovery of $Au(S_2O_3)_2^{3-}$ from thiosulfate leaching solutions.

CdS with hexagonal phase crystal structure possesses various surficial properties due to its different surface energy [31]. The changeable energy band structure would be driven by the variation of crystal structure, and then catalytic activity was modulated as well [32]. Based on the above discussions, CdS exhibited excellent light absorption capabilities, rich sulfur atoms and adjustable band structure, therefore it could achieve the efficient reduction-recovery of low-concentration Au $(S_2O_3)_2^{3-}$.

2. Materials and methods

2.1. Materials

The reagents used for preparing CdS including cadmium nitrate tetrahydrate ($Cd(NO_3)_2{\cdot}4H_2O$) and thiourea (CN_2H_4S, TU), were all acquired from Shanghai Macklin Biochemical Co., Ltd., China. Sodium sulfite (Na_2SO_3) was bought from Yunguan (Shanghai) Biotechnology Co., Ltd., China. Sodium thiosulfate pentahydrate ($Na_2S_2O_3{\cdot}5H_2O$), ammonium thiosulfate ($(NH_4)_2S_2O_3$), thioacetamide (CH_3CSNH_2, TAA) and ethanol absolute (C_2H_5OH) were obtained from Merck Life Science Technology (Nantong) Co., Ltd., China. Ethylenediamine ($C_2H_8N_2$, EDA) and sodium hydroxide (NaOH) were purchased from Sinopharm Chemical Reagent Co., Ltd., China. Hydrochloric acid (HCl) was obtained from Shanghai Aladdin Biochemical Technology Co., Ltd., China. N-BOC-L-Cysteine ($C_8H_{15}NO_4S$, L-Cys) was bought from Ningbo Haide Insu Biotechnology Co., Ltd., China. Standard gold solution ($HAuCl_4$, 1000 mg/L) of analytical grade was bought from Well Group Scientific Ltd., USA and used without further purification. Aqueous ammonia ($NH_3{\cdot}H_2O$) was gained from Dongguan Xunye Chemical Reagent Co., Ltd., China.

2.2. Samples preparation

In this experiment, CdS was prepared by the one-pot hydrothermal method. Cadmium ($Cd(NO_3)_2{\cdot}4H_2O$) and sulfur sources (L-cys) were added into mixed solution (20 ml EDA and 10 mL ultrapure water), being stirred for 30 min at 600 rpm. The above solution was placed in Teflon-lined stainless-steel autoclave and kept at 180 °C for 12 h. After cooling to room temperature, the obtained products were filtrated, washed with ultrapure water and ethanol, and dried at −60 °C in vacuum. First, we explored the effect of solvent by $Cd(NO_3)_2{\cdot}4H_2O$ (2 mmol), EDA and 67 % EDA (4 mmol), and the obtained samples were named as CdS-L-Cys-EDA, CdS-L-Cys-67%EDA. Then, effect of sulfur sources was investigated using $Cd(NO_3)_2{\cdot}4H_2O$ (3 mmol), TAA and TU (9 mmol), and corresponding samples were named as CdS-TAA and CdS-TU.

2.3. Experimental design

Adding $HAuCl_4$ into $(NH_4)_2S_2O_3$ solution was to prepare $Au(S_2O_3)_2^{3-}$ solution as described in previous works [33]. 5 mg CdS was added into 100 mL $Au(S_2O_3)_2^{3-}$ solution with concentration of 10 mg/L and reacted with stirring of 500 rpm at room temperature. At different time (0, 1, 2, 3, 5, 8, 10 h) intervals, certain amount of solution was extracted and filtered through 0.22 μm membrane for testing the concentration. Effects of environmental conditions including pH, initial concentration, light, catalyst dosage, and interferential ion on Au recovery were investigated. Concentration of Au was determined by an atomic absorption spectrometer (280Z AA, America).

Au recovery ability was evaluated by reduction capacity (R_e, mg/g) and recovery (R, %) by the following equations:

$$R_e = (C_0V_0 - CV)/m \quad (1)$$

$$R = \frac{C_0 - C}{C_0} \times 100\% \quad (2)$$

where C_0 and C were Au concentration before and after the reaction, respectively, mg/L; V_0 and V denote the volume of solution before and after the reaction, respectively, L; and m was the mass of the sample, g.

2.4. Material characterization

Phase, crystallinity, and preferred orientation of CdS were analyzed using X-ray diffraction (XRD) with Cu Kα (Bruker D8 ADVANCE, Germany). Micromorphology and element distribution on the surface of CdS were characterized using scanning electron microscopy (SEM, ZEISS Sigma 300, Germany) and transmission electron microscopy (TEM, JEOL JEM F200, Japan). X-ray photoelectron spectroscopy (XPS, K-Alpha, USA) was used to obtain the valence states of CdS before and after the reaction, while the atomic absorption spectrometer (280Z AA, USA) determined Au concentration in the solution. Raman spectroscopy analy (DXR, USA) based on helped analyze the molecular structure of CdS. To study surficial charges of solid–liquid interface, a Zeta potential analyzer (Zetasizer Nano ZS90) was used. Light adsorption ability was evaluated through UV−vis spectra (Shimadzu UV-3600 spectrophotometer, Japan). The optoelectronic properties of CdS were tested on a model VersaSTAT-450 electrochemical workstation in Princeton, USA. The fluorescence spectrophotometer (FLS1000, UK) tested the composite case of photogenerated carriers. Micromeritics ASAP 2460 automatic specific surface area and porosity analyzer (USA) was used to obtain the specific surface area and pore structure information.

3. Results and discussion

3.1. Characterization

Crystal and molecular structures were characterized by XRD and Raman test, as depicted in Fig. 1a, b. XRD patterns (Fig. 1a) showed that the peaks of CdS-L-Cys-EDA, CdS-L-Cys-67 %EDA, CdS-TAA and CdS-TU at 24.8°, 26.5°, 28.2°, 36.6°, 43.6°, 47.8°, 50.9°, 51.8°, 52.8°, and 66.8° were consistent with (1 0 0), (0 0 2), (1 0 1), (1 0 2), (1 1 0), (1 0 3), (2 0 0), (1 1 2), (2 0 1) and (2 0 3) facets of the hexagonal structural CdS standard cards (JCPDS 41-1049) [34,35], respectively. Specially, the related peak intensity of (0 0 2) in CdS-TU was highest, while lowest of that in CdS-Cys-EDA. Raman peaks at 300 cm^{-1} and 602 cm^{-1} (Fig. 1b) represented the first order (1 LO) and second order (2 LO) longitudinal optical phonon mode of CdS [36]. Red shift was due to the reduced crystal size under phonon constraint effect. The above results demonstrated the successful preparation of pure-phase CdS through adjusting various Cd and S sources.

Microscopic morphologies of CdS-L-Cys-67%EDA, CdS-TAA, and CdS-TU were characterized using SEM (Fig. 1c–e). CdS-L-Cys-67%EDA synthesized with L-cys displayed a structure composed of multiple short nanorods stacked together (Fig. 1c). In contrast, CdS-TAA prepared with thiourea revealed a distinct morphology with a few notably longer nanorods, attributing to its enhanced orientation along the (0 0 2) crystal plane (Fig. 1d). Longer the one-dimensional branched architecture is more beneficial for (0 0 2) facet exposing. As for CdS-TU, showcasing a different arrangement where unevenly lengthen short nanorods interlace (Fig. 1e). This unique formation potentially contributed to porous structure, thereby minimizing stacking, and enhancing the availability of active sites for photocatalytic reactions, ultimately augmenting the catalytic activity.

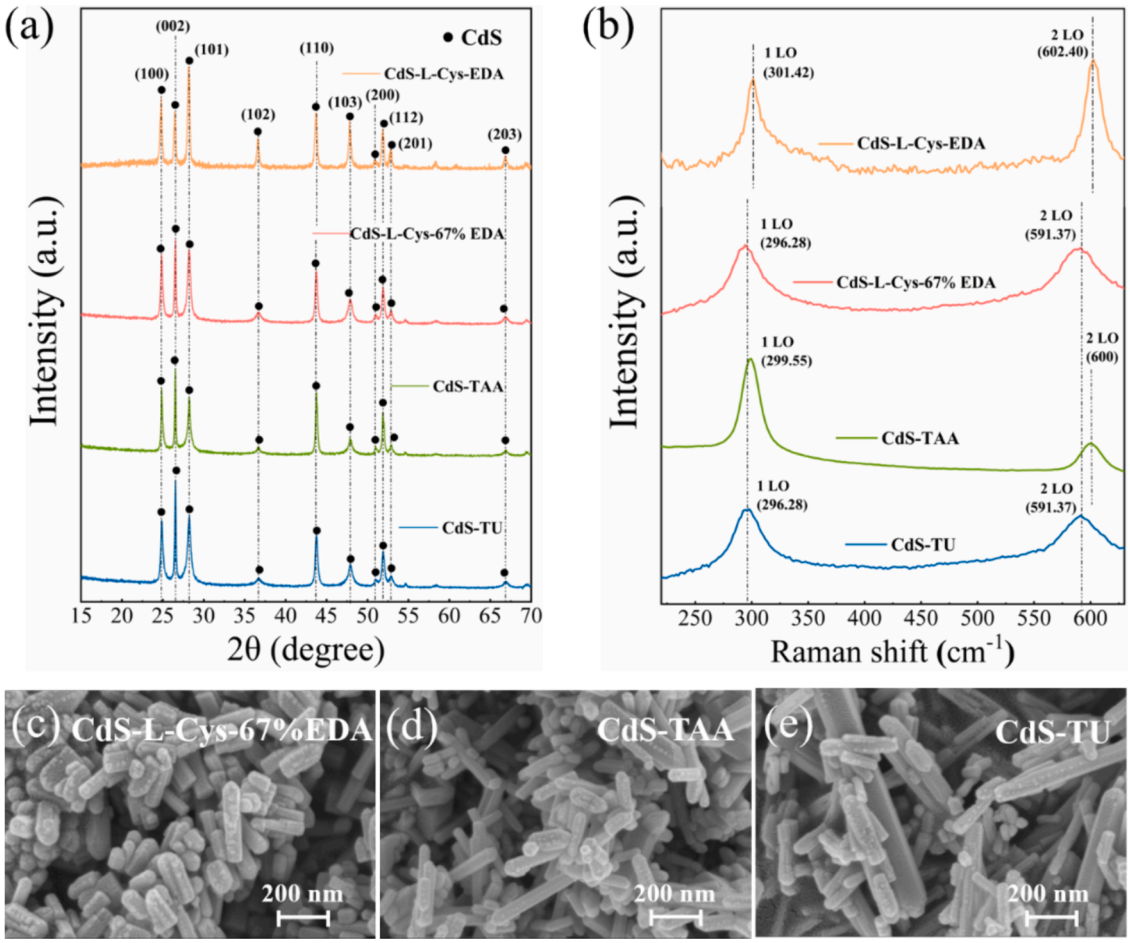

Fig. 1. XRD patterns (a) and Raman spectra (b) of CdS-L-Cys-EDA, CdS-L-Cys-67 %EDA, CdS-TAA and CdS-TU. SEM images of CdS-L-Cys-67 %EDA (c), CdS- TAA (d), and CdS-TU (e).

3.2. Recovery performances

To investigate Au recovery performances by CdS, various samples were applied on $Au(S_2O_3)_2^{3-}$ recovery in Fig. 2a. $Au(S_2O_3)_2^{3-}$ recovery quickly increased with the increased time. When time reached 8 h, CdS-TU had the maximum recovery of $Au(S_2O_3)_2^{3-}$ (98.62 %). Accordingly, the recovery rate using CdS-TU was the fastest in Fig. 2b. Studies have shown that by synthesizing CdS with a hexagonal, branched dendritic configuration in a TU solution, it is possible to achieve superior catalytic ability. This enhancement was attributed to one-dimensional branched architecture with more (002) facet exposing, smallest resistance to electron transfer across interfaces, and a conduction band bottom that is significantly more negative [37]. Therefore, CdS-TU was chosen for subsequent experiments to explore the feasibility of CdS in low-concentration $Au(S_2O_3)_2^{3-}$ recovery.

3.3. Effects of environmental conditions

Effect of light conditions on Au reduction-recovery performance was studied (Fig. 3a, b). It showed that the recovery (97.26 %) in the light condition was higher than that in dark condition (50.45 %), exhibiting that light played an important role in the reduction-recovery process.

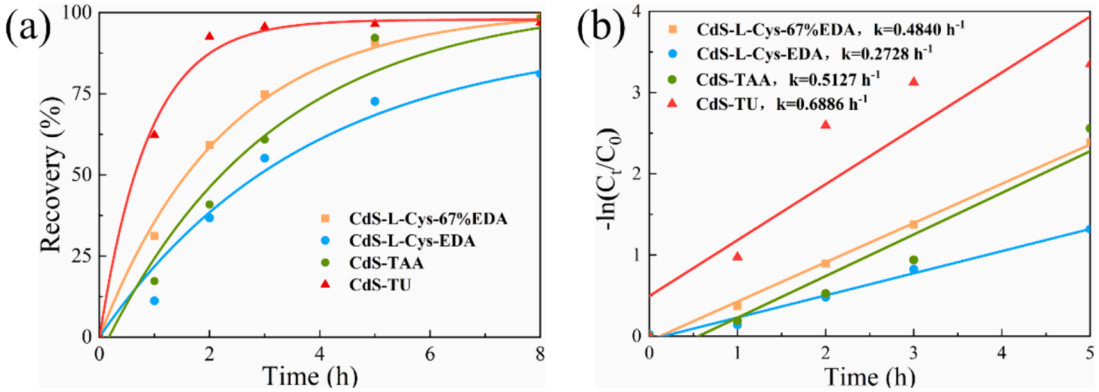

Fig. 2. $Au(S_2O_3)_2^{3-}$ recovery (a) and reaction rate (b) by CdS-L-Cys-EDA, CdS-L-Cys-67%EDA, CdS-TAA and CdS-TU.

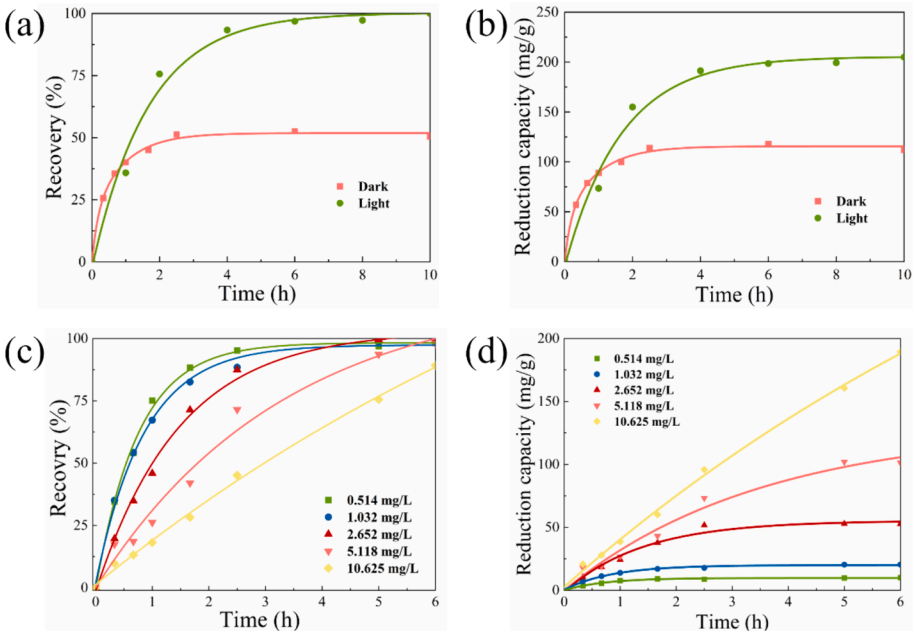

Fig. 3. Effect of environmental conditions on $Au(S_2O_3)_2^{3-}$ recovery: light (a, b), and initial concentration (c, d).

The related reduction capacity was up to 204.95 mg/g. Fig. 3c, d showed the recovery and reduction capacity of $Au(S_2O_3)_2^{3-}$ under various initial concentration ranges (from 0.514 mg/L to 10.625 mg/L). With increasing time, $Au(S_2O_3)_2^{3-}$ recovery revealed a sharp increase and then balance. Under the low initial concentration condition, recovery could achieve ~95 %. With the attraction of S atoms to gold complex, Au $(S_2O_3)_2^{3-}$ migrated to the surface of CdS by photoelectron reduction. When the initial concentration increased, immigration of $Au(S_2O_3)_2^{3-}$ would be gradually consumed by a reduction, thus exhibiting a high amount of gold recovery. The above results indicated that CdS had great potential in low-concentration $Au(S_2O_3)_2^{3-}$ recovery.

The solution pH not only affected the surface charges of material but also changed the content of H^+ and OH^-. Since stable solution environment for $Au(S_2O_3)_2^{3-}$ was alkaline, pH was considered from 8 to 12 (Fig. 4a). Recovery gradually increased as initial pH value of the solution increased. When reaching 10, $Au(S_2O_3)_2^{3-}$ recovery is the maximum (98.22 %). The result shown in Fig. 4b indicated that there are isoelectric points (between pH of 10 and 11) on CdS, and negatively charged CdS when pH was higher than 11. When pH is lower than 10, free anions ($S_2O_3^{2-}$) would compete with $Au(S_2O_3)_2^{3-}$ for the reactive sites on CdS through electrostatic interaction. As for pH of higher than 10, the $Au(S_2O_3)_2^{3-}$ recovery was slightly decreased. It was worth noting that under strong alkaline conditions, there was no electrostatic attraction between $Au(S_2O_3)_2^{3-}$ and CdS, which indicated that electrostatic interaction was not the main reason for $Au(S_2O_3)_2^{3-}$ adsorption. Moreover, $Au(S_2O_3)_2^{3-}$ recovery performance with various usage of materials was studied (Fig. 4c, d). With the increased usage, the Au $(S_2O_3)_2^{3-}$ recovery increased while oppositely in recovery capacity. It

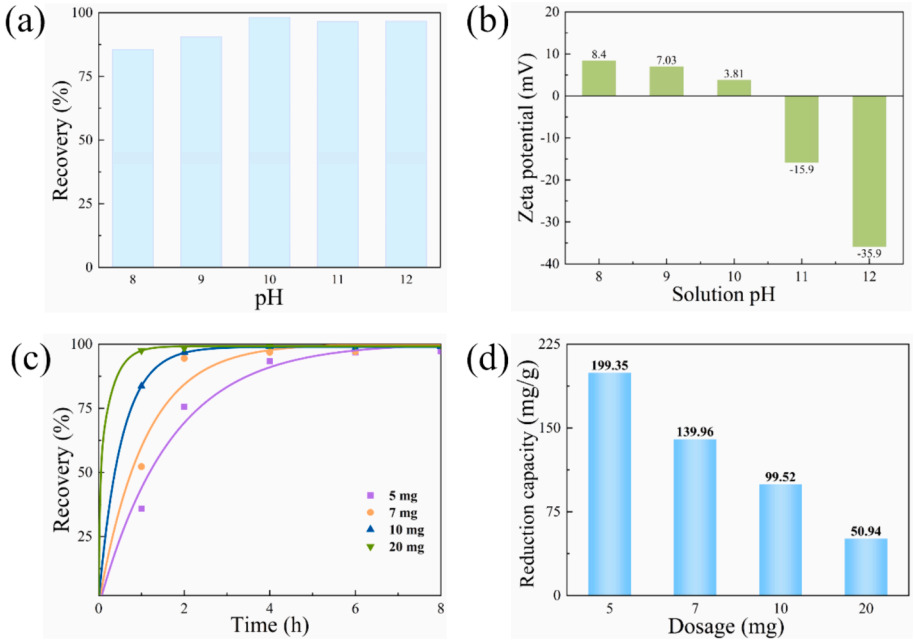

Fig. 4. Effect of environmental conditions on $Au(S_2O_3)_2^{3-}$ recovery: pH (a), and dosage of material (c, d) using CdS. Zeta potential of CdS (b).

indicated that little amount of CdS realized efficient Au recovery.

3.4. Existence of interferential ions

In the thiosulfate leaching process, thiosulfate and ammonia ions were excessively for better leaching gold [38], which would seriously affect the $Au(S_2O_3)_2^{3-}$ recovery, especially at a low concentration. As a main by-product of $S_2O_3^{2-}$, SO_3^{2-} would obviously affect the recovery performances [39]. Thus, we choose them as interferential ions to investigate the recovery performances in this section. With the aim of applying CdS in actual leaching solution, various concentrations of $S_2O_3^{2-}$ were added in $Au(S_2O_3)_2^{3-}$ solution. The recovery performances were recorded in Fig. 5a, b. More $S_2O_3^{2-}$ was added, and $Au(S_2O_3)_2^{3-}$ recovery decreased. This phenomenon originated from the competition of $S_2O_3^{2-}$ with $Au(S_2O_3)_2^{3-}$ on CdS. To some extent, Au recovery kept very high when the excess $S_2O_3^{2-}$ concentration was lower than 1.41 mg/L. SO_3^{2-} was one of the main oxidative decomposition products of $S_2O_3^{2-}$ [40]. In thiosulfate leaching process, it can be used as an additive to significantly improve the consumption of leaching reagent. Fig. 5c, d displayed the recovery ability of $Au(S_2O_3)_2^{3-}$ on CdS in the presence of different concentrations of SO_3^{2-}. $Au(S_2O_3)_2^{3-}$ recovery was influenced by various amounts of SO_3^{2-}, which might be due to the interaction between SO_3^{2-} and S within the CdS. However, its overall influence appears to be minimal [41]. Ammonia usually is added in thiosulfate leaching solutions to accelerate gold leaching rate [42]. Here, it was researched as an impact on the gold recovery, as shown in Fig. 5e, f. As increasing proportion of ammonia in solution, there was little influence on the recovery and reduction capacity. This was because the formation of ammonia was with positively charged, and couldn't compete with Au $(S_2O_3)_2^{3-}$ with negatively charged.

3.5. Au state after recovery

With the aim of investigating Au state after recovery, the chemical component was studied by XPS. In Fig. S1, XPS survey of CdS before and after recovery confirmed the existence of Au on CdS because of the appearance of Au characteristic peaks. Two characteristic diffraction peaks at 84.00 eV and 87.68 eV in XPS Au 4*f* spectrum (Fig. 6c) were ascribed to Au^0 [43], demonstrating that $Au(S_2O_3)_2^{3-}$ was recovered as the form of gold particles. Through comparing the result of XPS Cd 3*d* (411.97 and 411.99 eV, 405.23 and 405.25 eV) and S 2p (162.80 and 162.82 eV, 161.58 and 161.59 eV) [44] before and after reaction in Fig. 6a, b, the peaks changed little, which indicated that the reduction-recovery of $Au(S_2O_3)_2^{3-}$ was dominated by catalytic reduction.

Combined with the XRD result of CdS after recovery, it further demonstrated the Au state of gold particles. As displayed in Fig. 6d, the obvious new characteristic diffraction peaks at 38.2°, 44.5°, 64.6°, and 77.7° were ascribed to gold metal (111), (200), (220) and (311), respectively [45]. In addition, it was found that light was necessary in the reduction-recovery process because $Au(S_2O_3)_2^{3-}$ was reduced into gold particles through photoelectrons produced by CdS. Due to the small amount of gold particles under dark condition, it is hard to be detected in XRD result. So, we provided the XPS to reveal the Au state after recovery in Fig. S2. It is showed that the two peaks in Au 4f ascribing to

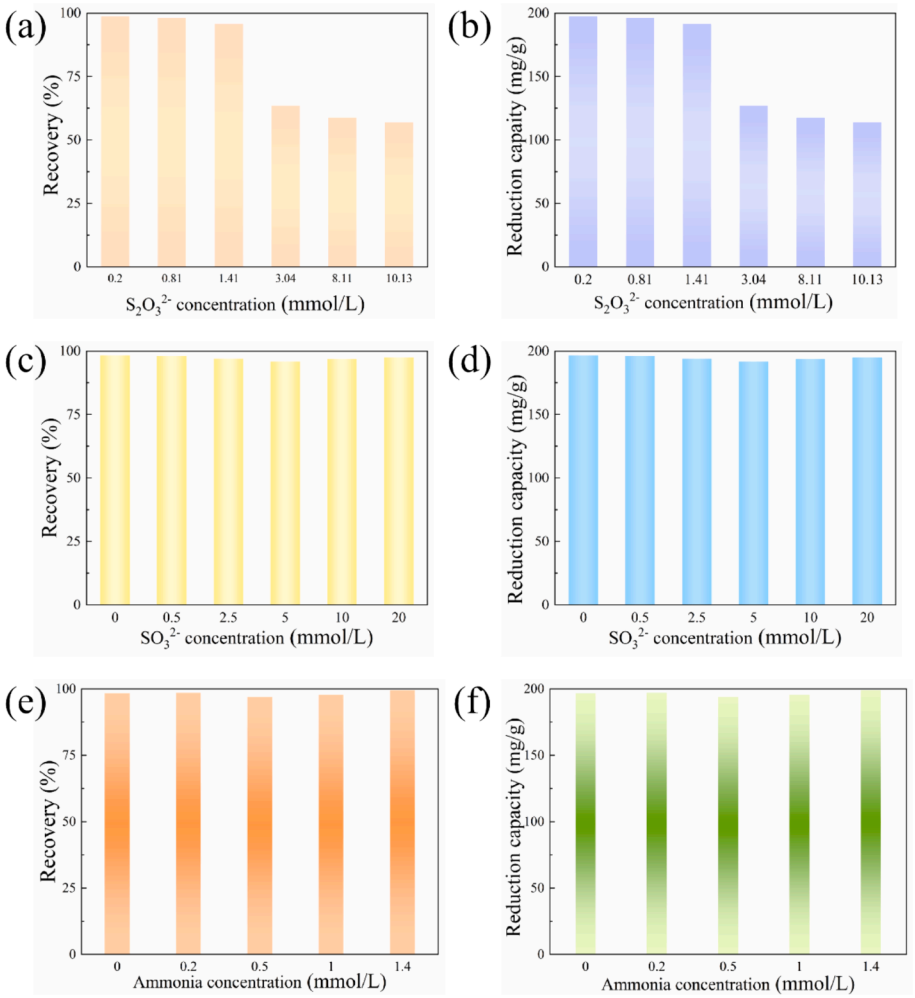

Fig. 5. Effect of $S_2O_3^{2-}$ (a, b), SO_3^{2-} (c, d), and ammonia (e, f) on the $Au(S_2O_3)_2^{3-}$ recovery and reduction capacity.

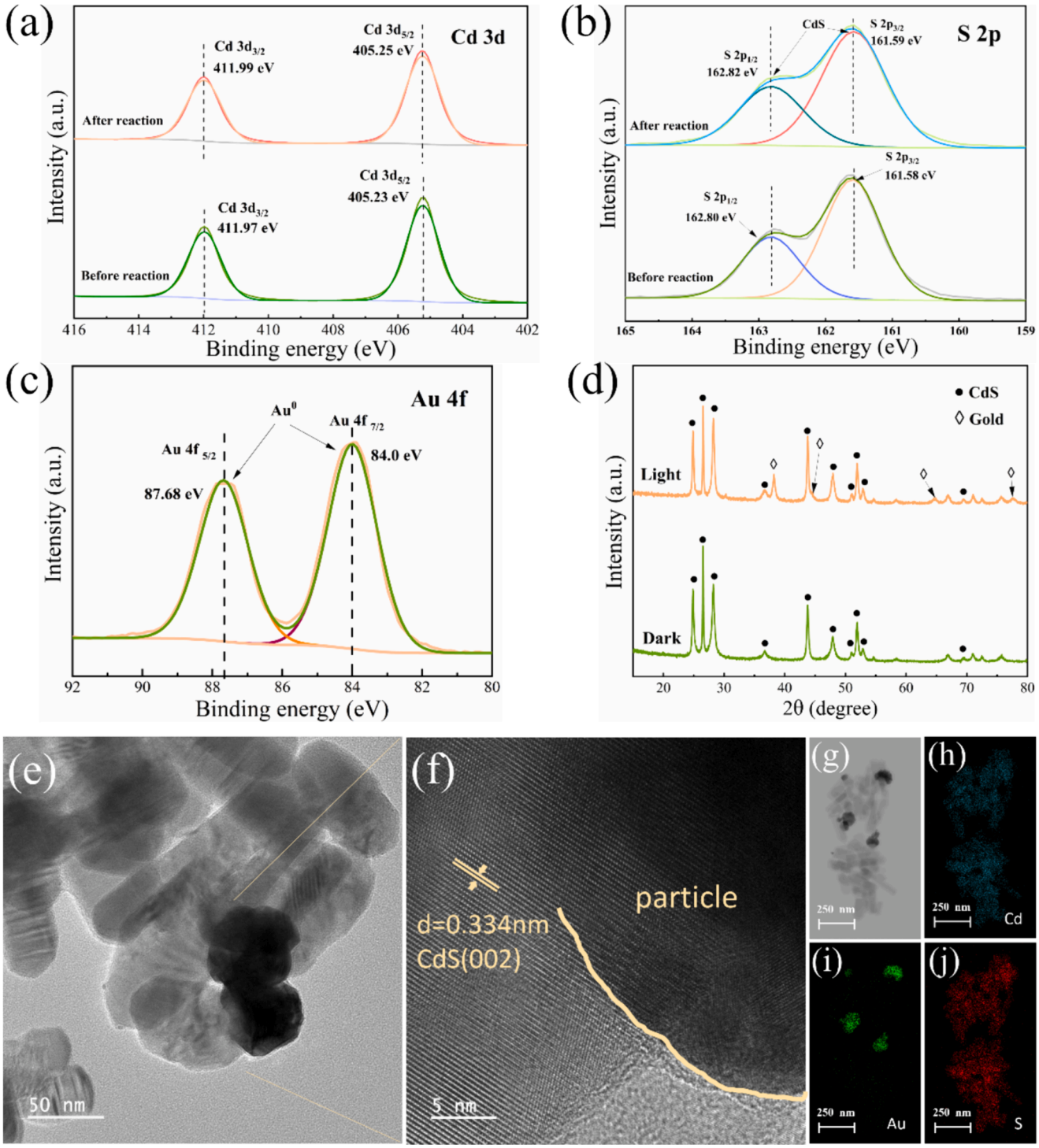

Fig. 6. The comparison of XPS spectrum of CdS-TU before and after reaction: Cd 3*d* spectrum (a), S 2*p* spectrum (b), the XPS spectrum of Au 4*f* (c), XRD patterns of CdS after $Au(S_2O_3)_2^{3-}$ recovery under dark and light (d), HR-TEM image (e, f), and EDS mapping (g-j) of CdS-TU after $Au(S_2O_3)_2^{3-}$ reduction-recovery.

Au^0 demonstrated the existence of chemical reduction. The instability of S on CdS [46] would reduce $Au(S_2O_3)_2^{3-}$ into gold particles as well.

TEM was used to analyze the morphology of CdS after recovery. As seen in Fig. S3 and Fig. 6e, the morphology was still nano-rods, and the lattice spacing of 0.334 nm was from (0 0 2) facet of CdS (Fig. 6f) [47]. Spherical nanoparticles with diameter of about 50 nm appeared and closely contacted with CdS. To determine the chemical composition of spherical particles, TEM corresponding mapping was analyzed (Fig. 6g–j). It revealed that the evenly distributed Cd and S elements on nano-rods CdS, while Au element was completely consistent with spherical particles. Based on the above discussions, the spherical particles were gold particles. Herein, low-concentration $Au(S_2O_3)_2^{3-}$ could be efficiently recovered in the form of gold particles by reduction-recovery method of CdS.

3.6. Mechanism for $Au(S_2O_3)_2^{3-}$ recovery by CdS

Fig. 7a presents the transient photocurrent response of CdS-L-Cys-EDA, CdS-L-Cys-67%EDA, CdS-TAA and CdS-TU under multi-cycle illumination. With the power source toggled between 30 and 60 s,

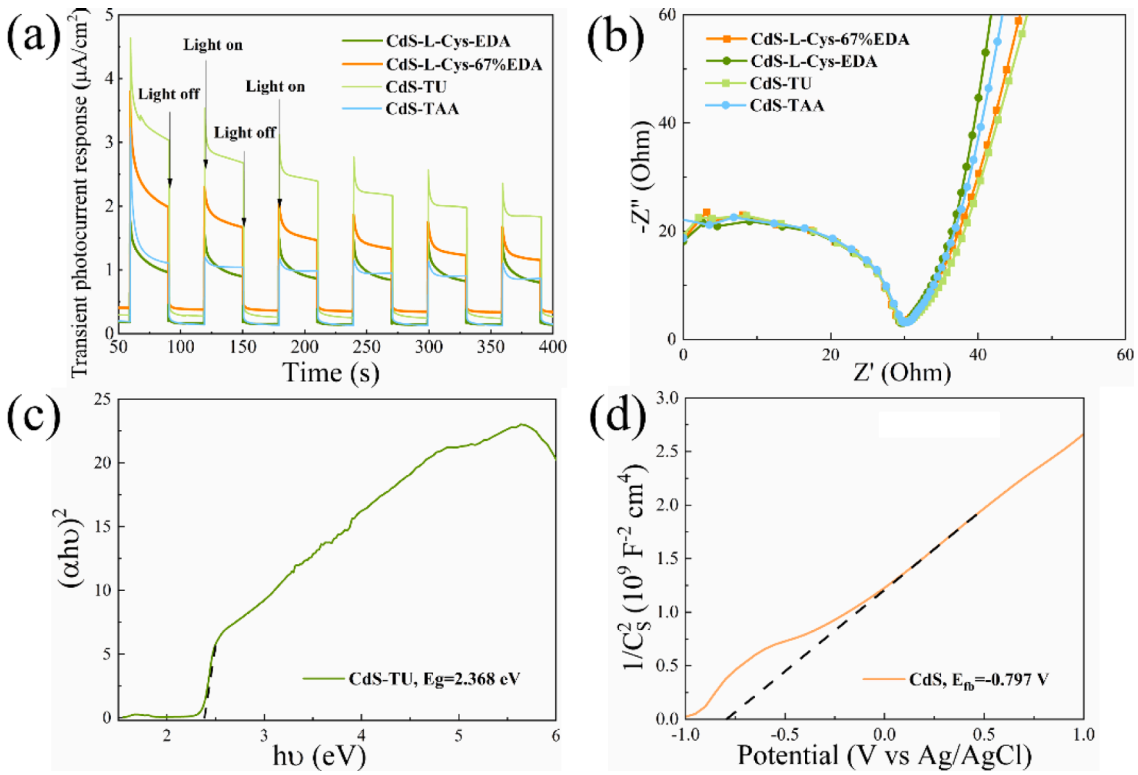

Fig. 7. Optical properties of CdS-L-Cys-EDA, CdS-L-Cys-67 %EDA, CdS-TAA and CdS-TU nanomaterials: transient photocurrent response (a), EIS impedance diagram (b), Tauc diagram (c), and Motto-Schottky diagram (d).

four samples exhibit photocurrent signals, indicating that all samples can generate photoelectrons. Compared to CdS-TU, the dynamic transient photocurrent response current values of CdS-L-Cys-EDA, CdS-L-Cys-67 %EDA and CdS-TAA are reduced. Therefore, CdS-TU, with a higher degree of (0 0 2) crystal plane orientation, produces more photogenerated carriers under light, which is more conducive to the separation of photogenerated electron-hole pairs. Electrochemical impedance spectroscopy (EIS) is operated to further investigate the effective separation and transport of photo-generated carriers in activated CdS-L-Cys-EDA, CdS-L-Cys-67%EDA, CdS-TAA and CdS-TU. The diameter of the semicircle in the high-frequency region shown in Fig. 7b directly reflects the resistance encountered in the charge transfer process. Ranked by diameter size and the consistent transient photocurrent response trend: CdS-L-Cys-67%EDA < CdS-L-Cys-EDA < CdS-TAA < CdS-TU, the overall difference among them is not significant, representing that all four samples maintain a similar level of performance in transporting photogenerated carriers.

The effective absorption of light was a key parameter for catalytic reaction by catalysis, and was given using UV–Vis spectrum (Fig. S4). It indicated that the absorption edge of CdS was around 530 nm, allowing the occurred reaction under natural light. Bandgap (E_g) was calculated using the Kubelka-Munk equation [48]:

$$(\alpha h\nu)^n = A(h\nu - E_g) \tag{3}$$

where α, h, ν, and A respectively represented the absorbance, Planck's constant ($6.62607015 \times 10^{-34}$ J/s), the frequency of light, and constant. The value of n was related to the type of electronic transition in the photocatalyst, with n = 2 for direct bandgap photocatalysts and n = 1/2 for indirect bandgap photocatalysts [49]. As calculated, CdS had a bandgap value of 2.368 eV (Fig. 7c).

Mott-Schottky analysis was utilized to examine flat band potential. The flat band potential (E_{fb}) of CdS was measured using the Mott-Schottky plot, which indicated a value of −0.797 V (vs. Ag/AgCl), as shown in Fig. 7d. Based on the Eqs. (4) and (5), the conduction band position of CdS was determined to be −0.810 eV, while the valence band potential was 1.558 eV (vs. NHE).

$$E(NHE) = E\left(\frac{Ag}{AgCl}\right) + 0.197 \tag{4}$$

$$E_{VB} = E_g + E_{CB} \tag{5}$$

where E_{CB} and E_{VB} respectively represented the conduction band edge and the valence band edge, $E(NHE)$ is the standard electrode potential, and $E\left(\frac{Ag}{AgCl}\right)$ is the electrode potential when the reference electrode is silver/silver chloride.

According to the above results, the mechanism for efficiently reducing and recovering $Au(S_2O_3)_2^{3-}$ using CdS was schematically shown in Fig. 8. Since $Au(S_2O_3)_2^{3-}$ was an anion, it could be rapidly adsorbed to the surface of CdS by electrostatic attraction. Besides, based on HASB theory, $Au(S_2O_3)_2^{3-}$ could bind strongly with the S atoms in CdS. The conduction band position of CdS (−0.810 eV) was lower than the redox potential of $Au(S_2O_3)_2^{3-}/Au^0$ (0.15 eV). When the incident photon energy was greater than the bandgap, $Au(S_2O_3)_2^{3-}$ could be reduced into gold particles on the surface of CdS. The possible chemical reaction was given as follows:

$$CdS + h\nu \rightarrow e^- + h^+ \tag{6}$$

$$e^- + Au(S_2O_3)_2^{3-} \rightarrow Au^0 + 2S_2O_3^{2-} \tag{7}$$

4. Conclusions

In the work, CdS with various exposed facets were prepared through adjusting sulfur sources in one-pot hydrothermal synthesis process. Au $(S_2O_3)_2^{3-}$ recovery by CdS obtained 98.62 % under low concentration condition, with a max reduction capacity of 204.95 mg/g. Low-concentration $Au(S_2O_3)_2^{3-}$ recovery by CdS was higher than 90 %. Au

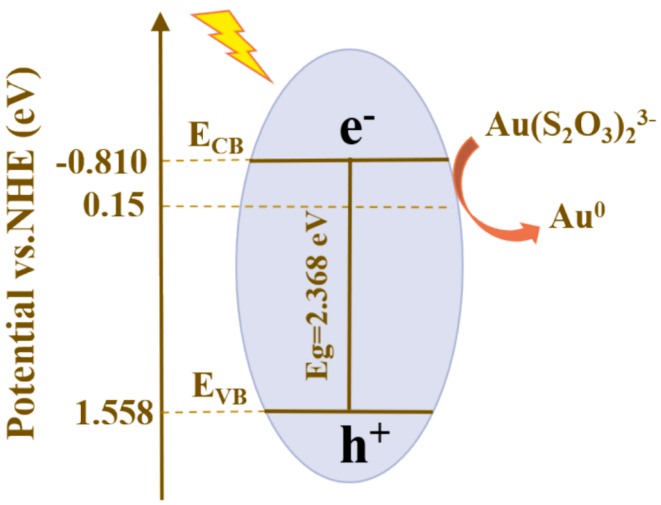

Fig. 8. The energy band structure of CdS and the mechanism of in-situ recovery of $Au(S_2O_3)_2^{3-}$.

$(S_2O_3)_2^{3-}$ was recovered on the surface of CdS as the form of gold metal. $Au(S_2O_3)_2^{3-}$ reduction was originated from catalytic and chemical reduction. Exposing more (0 0 2) facet in CdS facilitated the photocurrent intensity, which was beneficial for catalytic reduction of Au $(S_2O_3)_2^{3-}$. When pH was lower than a certain value, free anions ($S_2O_3^{2-}$) would compete with $Au(S_2O_3)_2^{3-}$ for the reactive sites on CdS through electrostatic interaction. As increased usage, $Au(S_2O_3)_2^{3-}$ recovery increased while oppositely in recovery capacity. In the presence of interfered ions, $Au(S_2O_3)_2^{3-}$ recovery was little affected. Thus, the work gives an insight into trace $Au(S_2O_3)_2^{3-}$ recovery to proceed the application of thiosulfate leaching in factories.

CRediT authorship contribution statement

Jiabei Gao: Writing – original draft, Validation, Methodology, Investigation. **Weiquan Zhan:** Writing – review & editing, Supervision, Data curation. **Ziwei Xiang:** Methodology, Investigation. **Shaoxian Song:** Investigation, Data curation. **José Luis Arauz-Lara:** Resources, Methodology. **Feifei Jia:** Methodology, Funding acquisition. **Peng Chen:** Writing – review & editing, Methodology.

Declaration of competing interest

The authors declare that they have no known competing financial interests or personal relationships that could have appeared to influence the work reported in this paper.

Data availability

Data will be made available on request.

Acknowledgements

The work is financially supported by the National Key Research and Development Program of China (2021YFC2900900), China Postdoctoral Science Foundation (2023M742726) and Postdoctoral Fellowship Program of CPSF (GZC20232016). Weiquan Zhan gratefully acknowledges the Consejo Nacional de Humanidades Ciencias y Tecnologías (CONAHCYT) of Mexico for offering him the scholarship under the grant No. 813934 during his Ph.D.

Appendix A. Supplementary data

Supplementary data to this article can be found online at https://doi.org/10.1016/j.molliq.2024.126018.

References

[1] W. Zhan, Q. He, X. Liu, Y. Guo, Y. Wang, L. Wang, Y. Guo, A.Y. Borisevich, J. Zhang, G. Lu, S. Dai, A sacrificial coating strategy toward enhancement of metal-support interaction for ultrastable Au nanocatalysts, J. Am. Chem. Soc. 138 (2016) 16130–16139, https://doi.org/10.1021/JACS.6B10472.
[2] M. Chen, S. Yamamuro, D. Farrell, S.A. Majetich, Gold-coated iron nanoparticles for biomedical applications, J. Appl. Phys. 93 (2003) 7551–7553, https://doi.org/10.1063/1.1555312.
[3] L. Reclaru, H. Lüthy, P.Y. Eschler, A. Blatter, C. Susz, Corrosion behaviour of cobalt-chromium dental alloys doped with precious metals, Biomaterials 26 (2005) 4358–4365, https://doi.org/10.1016/J.BIOMATERIALS.2004.11.018.
[4] R. Asmatulu, P.K. Bollavaram, V.R. Patlolla, I.M. Alarifi, W.S. Khan, Investigating the effects of metallic submicron and nanofilms on fiber-reinforced composites for lightning strike protection and EMI shielding, Adv. Compos. Hybrid Mater. 3 (2020) 66–83, https://doi.org/10.1007/S42114-020-00135-7.
[5] W. Eck, A.I. Nicholson, H. Zentgraf, W. Semmler, S. Bartling, Anti-CD_4-targeted gold nanoparticles induce specific contrast enhancement of peripheral lymph nodes in X-ray computed tomography of live mice, Nano Lett. 10 (2010) 2318–2322, https://doi.org/10.1021/NL101019S.
[6] C. Yue, H. Sun, W.J. Liu, B. Guan, X. Deng, X. Zhang, P. Yang, Environmentally benign, rapid, and selective extraction of gold from ores and waste electronic materials, Angew. Chem. – Int. Ed. 56 (2017) 9331–9335, https://doi.org/10.1002/ANIE.201703412.
[7] X. Xu, Y. Yang, X. Zhao, H. Zhao, Y. Lu, C. Jiang, D. Shao, J. Shi, Recovery of gold from electronic wastewater by Phomopsis sp. XP-8 and its potential application in the degradation of toxic dyes, Bioresour. Technol. 288 (2019) 121610, https://doi.org/10.1016/J.BIORTECH.2019.121610.
[8] H.E. Frimmel, Episodic concentration of gold to ore grade through Earth's history, Earth Sci. Rev. 180 (2018) 148–158, https://doi.org/10.1016/J.EARSCIREV.2018.03.011.
[9] X. Zeng, J.A. Mathews, J. Li, Urban mining of E-waste is becoming more cost-effective than virgin mining, Environ. Sci. Tech. 52 (2018) 4835–4841, https://doi.org/10.1021/ACS.EST.7B04909.
[10] G. Deschênes, Advances in the cyanidation of gold, Dev. Mineral Process. 15 (2005) 479–500, https://doi.org/10.1016/S0167-4528(05)15020-0.
[11] Y. Kianinia, M.R. Khalesi, M. Abdollahy, G. Hefter, G. Senanayake, L. Hnedkovsky, A.K. Darban, M. Shahbazi, Predicting cyanide consumption in gold leaching: a kinetic and thermodynamic modeling approach, Minerals 8 (2018) 110, https://doi.org/10.3390/MIN8030110.
[12] K. Li, Q. Li, Y. Zhang, X. Liu, Y. Yang, T. Jiang, Improved thiourea leaching of gold from a gold ore using additives, Hydrometall. 222 (2023) 106204, https://doi.org/10.1016/J.HYDROMET.2023.106204.
[13] I. Korolev, P. Altınkaya, P. Halli, P.M. Hannula, K. Yliniemi, M. Lundström, Electrochemical recovery of minor concentrations of gold from cyanide-free cupric chloride leaching solutions, J. Clean. Prod. 186 (2018) 840–850, https://doi.org/10.1016/J.JCLEPRO.2018.03.177.
[14] H. Li, E. Oraby, J. Eksteen, T. Mali, Extraction of gold and copper from flotation tailings using glycine-ammonia solutions in the presence of permanganate, Minerals 12 (2022) 1153–1157, https://doi.org/10.3390/MIN12050612.
[15] Q. Wang, X. Hu, F. Zi, P. Yang, Y. Chen, S. Chen, Environmentally friendly extraction of gold from refractory concentrate using a copper – ethylenediamine – thiosulfate solution, J. Clean. Prod. 214 (2019) 860–872, https://doi.org/10.1016/J.JCLEPRO.2019.01.007.
[16] Q. Weng, S. Song, W. Zhan, X. Zhang, Z. Xiang, J. Gao, F. Jia, Novel recovery of a low-concentration gold thiosulfate complex through electroreduction via a walnut shell charcoal electrode, Green Smart Min. Eng. 1 (2024) 58–66, https://doi.org/10.1016/J.GSME.2024.03.004.
[17] J. Wang, F. Xie, Y. Pan, W. Wang, Leaching of gold with copper-citrate-thiosulfate solutions, Miner. Process. Extr. Metall. Rev. 43 (2022) 916–925, https://doi.org/10.1080/08827508.2021.1969389.
[18] Y. Lin, X. Hu, F. Zi, Y. Chen, S. Chen, X. Li, L. Zhao, Y. Li, Synergistical thiourea and thiosulfate leaching gold from a gold concentrate calcine with copper-ammonia catalysis, Sep. Purif. Technol. 327 (2023) 124928, https://doi.org/10.1016/J.SEPPUR.2023.124928.
[19] J. Chen, F. Xie, W. Wang, Y. Fu, J. Wang, Leaching of gold and silver from a complex sulfide concentrate in copper-tartrate-thiosulfate solutions, Metals (Basel) 12 (2022) 1152, https://doi.org/10.3390/MET12071152.
[20] M.G. Aylmore, D.M. Muir, Thiosulfate leaching of gold - a review, Miner. Eng. 14 (2001) 135–174, https://doi.org/10.1016/S0892-6875(00)00172-2.
[21] N.R. Das, S.N. Bhattacharyya, Solvent extraction of gold, Talanta 23 (1976) 535–540, https://doi.org/10.1016/0039-9140(76)80151-8.
[22] B.R. Green, M.H. Kotze, J.P. Wyethe, Developments in ion exchange: the Mintek perspective, JOM 54 (2002) 37–43, https://doi.org/10.1007/BF02709220.
[23] W.L. Choo, M.I. Jeffrey, An electrochemical study of copper cementation of gold(I) thiosulfate, Hydrometallurgy 71 (2004) 351–362, https://doi.org/10.1016/S0304-386X(03)00087-2.
[24] A. Sheel, D. Pant, Recovery of gold from electronic waste using chemical assisted microbial biosorption (hybrid) technique, Bioresour. Technol. 247 (2018) 1189–1192, https://doi.org/10.1016/J.BIORTECH.2017.08.212.
[25] T.H. Bui, W. Lee, S.B. Jeon, K.W. Kim, Y. Lee, Enhanced Gold(III) adsorption using glutaraldehyde-crosslinked chitosan beads: effect of crosslinking degree on

adsorption selectivity, capacity, and mechanism, Sep. Purif. Technol. 248 (2020) 116989, https://doi.org/10.1016/J.SEPPUR.2020.116989.
[26] S. Zeng, F. Jia, B. Yang, S. Song, In-situ reduction of gold thiosulfate complex on molybdenum disulfide nanosheets for a highly-efficient recovery of gold from thiosulfate solutions, Hydrometallurgy 195 (2020) 105369, https://doi.org/10.1016/J.HYDROMET.2020.105369.
[27] W. Zhan, X. Zhang, Y. Yuan, Q. Weng, S. Song, M. de J. Martínez-López, J.L. Arauz-Lara, F. Jia, Regulating chemisorption and electrosorption activity for efficient uptake of rare earth elements in low concentration on oxygen-doped molybdenum disulfide, ACS Nano 18 (2024) 7298–7310, https://doi.org/10.1021/ACSNANO.4C00691.
[28] D. Zhang, L. Liu, L. Zhang, K. Qi, H. Zhang, X. Cui, An anti-photocorrosive photoanode based on a CdS/Ni_xS_y @NF heterostructure for visible-light-driven water splitting, Appl. Surf. Sci. 420 (2017) 161–166, https://doi.org/10.1016/J.APSUSC.2017.05.144.
[29] Z. Da Meng, L. Zhu, J.G. Choi, C.Y. Park, W.C. Oh, Sonocatalytic degradation of Rhodamine B in the presence of C_{60} and CdS coupled TiO_2 particles, Ultrason. Sonochem. 19 (2012) 143–150, https://doi.org/10.1016/J.ULTSONCH.2011.05.006.
[30] W. Zhan, Y. Yuan, X. Yao, B. Yang, F. Jia, C. Lin, J.L. Arauz-Lara, S. Song, Efficient recovery of gold(I) from thiosulfate solutions through photocatalytic reduction with Mn(II)-doped MoS_2, ACS Sustain. Chem. Eng. 9 (2021) 11681–11690, https://doi.org/10.1021/ACSSUSCHEMENG.1C02160.
[31] T. Chen, W. Chen, Z. Zhang, X. Jiang, M.S. Javed, M. Xie, W. Han, Preferential photo-carrier exchange in (010) facet of $BiVO_4$ with decorated CdS nanoparticles, Appl. Phys. Lett. 119 (2021) 253902, https://doi.org/10.1063/5.0075219.
[32] X. Yang, B. Wang, Y. Mu, M. Zheng, Y. Wang, Photocatalytic performance of cubic and hexagonal phase CdS synthesized via different Cd sources, J. Electron. Mater. (2019) 2895–2901, https://doi.org/10.1007/S11664-019-06967-4.
[33] W. Zhan, Y. Yuan, B. Yang, F. Jia, S. Song, Construction of MoS_2 nano-heterojunction via ZnS doping for enhancing in-situ photocatalytic reduction of gold thiosulfate complex, Chem. Eng. J. 394 (2020) 124866, https://doi.org/10.1016/J.CEJ.2020.124866.
[34] N. Soltani, E. Saion, M.Z. Hussein, M. Erfani, A. Abedini, G. Bahmanrokh, M. Navasery, P. Vaziri, Visible light-induced degradation of methylene blue in the presence of photocatalytic ZnS and CdS nanoparticles, Int. J. Mol. Sci. 13 (2012) 12242–12258, https://doi.org/10.3390/IJMS131012242.
[35] L. Wang, Z. Liu, J. Han, R. Li, M. Huang, Stepwise synthesis of Au@CdS-CdS nanoflowers and their enhanced photocatalytic properties, Nanoscale Res. Lett. 14 (2019) 148, https://doi.org/10.1186/S11671-019-2977-Z.
[36] A. Giugni, G. Das, A. Alabastri, R.P. Zaccaria, M. Zanella, I. Franchini, E. Di Fabrizio, R. Krahne, Optical phonon modes in ordered core-shell CdSe/CdS nanorod arrays, Phys. Rev. B: Condens. Matter Mater. Phys. 85 (2012) 115413, https://doi.org/10.1103/PHYSREVB.85.115413.
[37] H. Li, L. Liu, Z. Wang, X. Zheng, S. Meng, S. Chen, X. Fu, Optimizing the precursor of sulfur source for hydrothermal synthesis of high performance CdS for photocatalytic hydrogen production, RSC Adv. 8 (2018) 11489–11497, https://doi.org/10.1039/C8RA00250A.
[38] P.Z. Xiang, Q. Liu, C. Deng, G.H. Ye, Electrochemical analysis of the dissolution of gold in a copper-ethylenediamine-thiosulfate system, Green Process. Synth, 12 (2023) 265–271, https://doi.org/10.1515/GPS-2022-8133.
[39] X. Zhang, W. Zhan, Q. Weng, S. Wang, S. Song, J.L. Arauz-Lara, F. Jia, Electro reduction-recovery of $Au(S_2O_3)_2^{3-}$ within a low concentration range via multi-porous activated carbon electrodes, Sep. Purif. Technol. 354 (2025) 129134, https://doi.org/10.1016/J.SEPPUR.2024.129134.
[40] A.J. Findlay, A. Kamyshny, Turnover rates of intermediate sulfur species (S_x^{2-}, S_0, $S_2O_3^{2-}$, $S_4O_6^{2-}$, SO_3^{2-}) in anoxic freshwater and sediments, Front. Microbiol. 8 (2017) 2551, https://doi.org/10.3389/FMICB.2017.02551.
[41] X.Y. Chen, X.Z. Lan, Q.L. Zhang, J. Zhou, Y.H. Song, Behavior of $S_2O_3^{2-}$ and SO_3^{2-} in sulfur-bearing aqueous solution system for gold leaching, Trans. Nonferrous Metals Soc. China (English Ed.) 20 (2010) s46–s49, https://doi.org/10.1016/S1003-6326(10)60010-6.
[42] B. Xu, K. Li, Z. Dong, Y. Yang, Q. Li, X. Liu, T. Jiang, Eco-friendly and economical gold extraction by nickel catalyzed ammoniacal thiosulfate leaching-resin adsorption recovery, J. Clean. Prod. 233 (2019) 1475–1485, https://doi.org/10.1016/J.JCLEPRO.2019.06.182.
[43] I.S. Zhidkov, E.Z. Kurmaev, S.O. Cholakh, E. Fazio, L. D'Urso, XPS study of interactions between linear carbon chains and colloidal Au nanoparticles, Mendeleev Commun. 30 (2020) 285–287, https://doi.org/10.1016/J.MENCOM.2020.05.007.
[44] Mohamed Nawfal Ghazzal, Robert Wojcieszak, Gijo Raj, Eric M. Gaigneaux, Study of mesoporous CdS-quantum-dot-sensitized TiO_2 films by using X-ray photoelectron spectroscopy and AFM, Beilstein J. Nanotechnol. 5 (2014) 68–76, https://doi.org/10.3762/bjnano.5.6.
[45] P. Singh, K. Kumari, A. Katyal, R. Kalra, R. Chandra, Synthesis and characterization of silver and gold nanoparticles in ionic liquid, Spectrochim. Acta A Mol. Biomol. Spectrosc. 73 (2009) 218–220, https://doi.org/10.1016/J.SAA.2009.02.007.
[46] J. Zhang, X. Yuan, M. Si, L. Jiang, H. Yu, Core-shell structured cadmium sulfide nanocomposites for solar energy utilization, Adv. Colloid Interface Sci. 282 (2020) 102209, https://doi.org/10.1016/J.CIS.2020.102209.
[47] A. Phuruangrat, T. Thongtem, S. Thongtem, Effect of Cd and S sources on the morphologies of CdS synthesized by solvothermal reactions in mixed solvents, Curr. Appl Phys. 9 (2009) 201–204, https://doi.org/10.1016/J.CAP.2009.01.041.
[48] S.K. Abdel-Aal, M.F. Kandeel, A.F. El-Sherif, A.S. Abdel-Rahman, Synthesis, characterization, and optical properties of new organic–inorganic hybrid perovskites $[(NH_3)_2(CH_2)_3]CuCl_4$ and $[(NH_3)_2(CH_2)_4]CuCl_2Br_2$, Phys. Status Solidi (A) Appl. Mater. Sci. 218 (2021) 2100036, https://doi.org/10.1002/PSSA.202100036.
[49] S. Parameswaran, R. Bakkiyaraj, P. Shanmugam, T. Venugopal, Solid combustion synthesis of MnO_2/NiO/Ag nanocomposites for efficient degradation of methylene blue and their antibacterial activity, Chem. Phys. 575 (2023) 112077, https://doi.org/10.1016/J.CHEMPHYS.2023.112077.